analytical chemistry

pubs.acs.org/ac

Article

LipidA-IDER to Explore the Global Lipid A Repertoire of Drug-Resistant Gram-Negative Bacteria

Xue Li Guan,* Johnathan Yi-Xiong Loh, Marco Lizwan, Sharon Cui Mun Chan, Jeric Mun Chung Kwan, Tze Peng Lim, Tse Hsien Koh, Li-Yang Hsu, and Bernett Teck Kwong Lee

Cite This: *Anal. Chem.* 2023, 95, 602−611

Read Online

ACCESS | Metrics & More | Article Recommendations | Supporting Information

ABSTRACT: With the global emergence of drug-resistant bacteria causing difficult-to-treat infections, there is an urgent need for a tool to facilitate studies on key virulence and antimicrobial resistant factors. Mass spectrometry (MS) has contributed substantially to the elucidation of the structure-function relationships of lipid A, the endotoxic component of lipopolysaccharide which also serves as an important protective barrier against antimicrobials. Here, we present LipidA-IDER, an automated structure annotation tool for system-level scale identification of lipid A from high-resolution tandem mass spectrometry (MS^2) data. LipidA-IDER was validated against previously reported structures of lipid A in the reference bacteria, *Escherichia coli* and *Pseudomonas aeruginosa*. Using MS^2 data of variable quality, we demonstrated LipidA-IDER annotated lipid A with a performance of 71.2% specificity and 70.9% sensitivity, offering greater accuracy than existing lipidomics software. The organism-independent workflow was further applied to a panel of six bacterial species: *E. coli* and Gram-negative members of ESKAPE pathogens. A comprehensive atlas comprising 188 distinct lipid A species, including remodeling intermediates, was generated and can be integrated with software including MS-DIAL and Metabokit for identification and semiquantitation. Systematic comparison of a pair of polymyxin-sensitive and polymyxin-resistant *Acinetobacter baumannii* isolated from a human patient unraveled multiple key lipid A structural features of polymyxin resistance within a single analysis. Probing the lipid A landscape of bacteria using LipidA-IDER thus holds immense potential for advancing our understanding of the vast diversity and structural complexity of a key lipid virulence and antimicrobial-resistant factor. LipidA-IDER is freely available at https://github.com/Systems-Biology-Of-Lipid-Metabolism-Lab/LipidA-IDER.

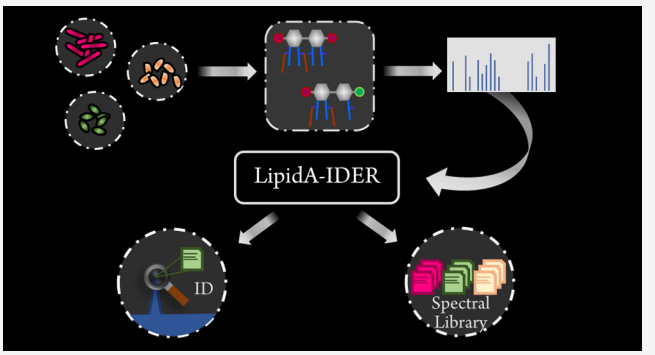

Gram-negative bacteria are protected from their environment by a unique and structurally complex dual bilayer membrane architecture. Lipopolysaccharides (LPS), the major component of the outer membrane, function as a permeability barrier against antimicrobials and are a key virulence factor.[1−3] LPS comprise three distinct regions: a highly variable O-antigen domain, a glycan core, and a hydrophobic glycolipid, termed lipid A. Lipid A is further defined by its distinct diglucosamine backbone which can be substituted by fatty acyls (FAs) at four positions (2, 3, 2′, and 3′ carbons) and modified at two positions (1 and 4′ carbons) with headgroups, including phosphate, phosphoethanolamine (PEtN), hexosamine (HexN), and 4-amino-4-deoxy-L-arabinose (Ara4N).[4,5] Less common variants, including the presence of unusual 2-amino-2-deoxy-gluconate and 2,3-diamino-2,3-dideoxyglucose moieties in the sugar backbone,[6,7] exist. Structural variations of lipid A strongly influence its interactions with host receptors and consequently the potency of the immune response it elicits.[8−10] Furthermore, lipid A remodeling is one of the key mechanisms of resistance to cationic antimicrobial peptides, including polymyxins (PMXs).[4] Development of antimicrobials that target this lipid A[11−13] and the use of modified lipid A as potential vaccine adjuvants[14,15] continue to be promising avenues for therapeutic interventions against Gram-negative bacterial infections. Comprehensive characterization of lipid A is hence critical for understanding its structure-function relationships in the context of virulence, antimicrobial resistance (AMR), and therapeutic designs.

With the development of data-dependent acquisition (DDA)[16] and data-independent acquisition (DIA),[17] comprehensive structural characterization of lipids, including lipid A, using tandem mass spectrometry (MS^2) can be performed in a simultaneous fashion within a single analysis. Interpretation of tandem mass spectra is, however, a manual process which typically requires expert understanding of the fragmentation

Received: August 19, 2021
Accepted: December 5, 2022
Published: January 4, 2023

https://doi.org/10.1021/acs.analchem.1c03566
Anal. Chem. 2023, 95, 602−611

pathways. To keep up with the rapid data acquisition rates enabled by modern MS^2 technologies, significant advances have been made in the development of computational tools for data deconvolution and MS^2-based compound identifications.[17−22] Automated lipid identification capitalizes on the predictable nature of fragmentations for similar molecules within each lipid subclass. Two common identification strategies used in lipidomics include (i) spectra matching against a database derived from experimental data and/or *in silico* computation,[18,23−26] and (ii) decision tree based on fragmentation rules.[19] However, existing lipid identification pipelines have limited utility for lipid A analyses, in part due to the lack of spectral databases. Moreover, analysis of lipid A is technically challenging due to its vast diversity and structural complexity.

Two lipid A-specific workflows for automation of lipid A structure identification, hierarchical tandem mass spectrometry (HiTMS)[27] and UVliPiD,[28] were designed for MS^n data generated using linear ion-trap MS, with the latter employing ultraviolet photo- dissociation collision-induced dissociation (UVPDCID)[29], a novel hybrid dissociation technique. These methods are extremely powerful for detailed structural assignments of lipid A, including localization of modifications. However, access to these technologies, particularly UVPD, is limited. Moreover, the algorithm for HiTMS is built on a bacterial species-specific signature ion database and will require further expansion to broaden its coverage.

To enable global profiling of lipid A from diverse biological origins, a structure identification workflow should be scalable, robust, and easily adopted by nonspecialists for spectral interpretations. Hence, LipidA-IDER was developed with a fragmentation-rule-based approach to assign lipid A identities for high-resolution MS^2 data. Using LipidA-IDER, we characterized 218 potential lipid A species (188 distinct structures) across the model organism, *E. coli*, and the Gram-negative members of ESKAPE pathogens: *Enterobacter* species, *Klebsiella pneumoniae*, *Pseudomonas aeruginosa*, and *Acinetobacter baumannii*.[28] This is the first systematic and comprehensive atlas detailing the lipid A landscape of ESKAPE-a group of nosocomial pathogens classified by the World Health Organization as priority pathogens due to their rapid emergence of AMR and associated mortality risks.[30] In addition, multiple structural signatures of PMX-resistant *A. baumannii* were defined, corroborating observations from past genetics and biochemical studies.[31−33] With LipidA-IDER, we further generated an experimentally derived reference spectral library that can be integrated with other common lipidomic pipelines, including MS-DIAL[26] and MetaboKit,[25] for spectral similarity-based identification and semiquantitative analyses of these characterized lipid A, which will facilitate future structure-function studies.

EXPERIMENTAL SECTION

Analytical Reagents and Lipid A Standards. Methanol (LC−MS grade) and chloroform (spectroscopy grade) were from Thermo Fisher Scientific, and Tedia, respectively. Ammonium hydroxide solution and mono- and diphosphorylated lipid A from *E. coli* F583 Rd mutant were from Sigma-Aldrich.

Bacterial Strains and Culture. Bacterial species and strains used in this study and their sources are summarized in the Supporting Information Methods. Cultures were grown overnight in lysogeny broth (LB) (Difco) at 37 °C with shaking at 150 rpm, and subsequently inoculated at a starting optical density (600 nm) of 0.05 in LB. Stationary phase bacteria were collected by centrifugation at 3000*g* at 4 °C for 10 min, followed by washing with phosphate-buffered saline. Samples were snap frozen in liquid nitrogen and stored at −80 °C.

Extraction of Lipopolysaccharides (LPS). LPS were extracted by a modified Bligh and Dyer method.[34] Briefly, chloroform/methanol (1/2, volume/volume (v/v)) was added to the bacterial pellet, followed by incubation for 4 hours at 4 °C, with shaking. Water and chloroform were added, and the samples were centrifuged for 15 min at 4 °C, 2000*g*. The upper aqueous layer was collected, re-extracted twice with chloroform, and dried.

Acid Hydrolysis of LPS and Extraction of Lipid A. A modified method described by Caroff et al was used.[35] The dried aqueous phase fraction from LPS extraction was resuspended in 12.5 mM sodium acetate with 1% sodium dodecyl sulfate (pH 4.5) (Sigma-Aldrich). Samples were sonicated for 10 min, followed by incubation at 100 °C for 40 min. After allowing the samples to cool, chloroform/methanol (1:1, v/v) was added, followed by centrifugation at 2000*g* for 15 min at 4 °C. The organic phase was collected and re-extracted with artificial upper phase (chloroform/methanol/water (2/2/1.8, v/v/v)). The organic fraction was dried under a stream of nitrogen and stored at −80 °C.

Liquid Chromatography and Mass Spectrometry (LC−MS) Analysis. Mass spectrometry (MS) and tandem MS (MS^2) analyses of lipid A were performed using a SCIEX TripleTOF 6600 quadrupole time-of-flight (qToF) mass spectrometer in the negative electrospray ionization (ESI) mode. Lipid A were separated by liquid chromatography (Agilent 1290) using an Inertsil SIL column (3 μm, 2.1 × 150 mm, GL Sciences, Japan). The mobile phase A consisted of chloroform/methanol/ammonium hydroxide (80/19.5/0.5, v/v/v) and B consisted of chloroform/methanol/water/ammonium hydroxide (40/50/9.5/0.5, v/v/v/v). The gradient with a flow rate of 0.25 mL/min started with 5% mobile phase B held for 2 min. The composition of mobile phase B was then increased to 70% over 6 min and to 99% over 5 min. Mobile phase B was then held at 99% for 1 min, followed by re-equilibration. Automated MS^2 analyses were performed in the information dependent acquisition (IDA) mode with the top 20 ions selected per scan for fragmentation and without exclusion time. MS^2 was focused on $[M - H]^-$ ions to systematically characterize lipid A, considering most lipid A can form singly charged ions. Collision energy (CE) from 40 to 120 V, with steps of 10 V, was applied to generate the fragmentation profiles of lipid A for all samples (purified *E. coli* lipid A fractions and biological extracts). For all biological extracts, CE 40, 60, 90, and 110 V were used in the second analytical batch, and CE 90 and 110 V were used in the third analytical batch. Biological replicates were analyzed in the IDA mode (CE 110 V) and targeted product ion scans (with various CE) were performed for low abundant lipid A.

To determine the reproducibility of LipidA-IDER, *E. coli* F583 Rd mutant monophosphorylated fraction was analyzed in four independent analytical batches, each with at least four technical replicates. For relative quantitation of lipid A, samples (two biological replicates, with three technical triplicates) were analyzed with two LC−MS technical replicates. Quality control (QC) samples comprising pooled samples were included.

LipidA-IDER Workflow and Availability. LipidA-IDER is freely available at https://github.com/Systems-Biology-Of-Lipid-Metabolism-Lab/LipidA-IDER. The workflow is coded

https://doi.org/10.1021/acs.analchem.1c03566
Anal. Chem. 2023, 95, 602−611

using Python, and the fragmentation patterns were derived from data generated in this study and detailed literature review (Supporting Information Tables S2−S3). Raw .wiff files were converted to .ms2 format with ProteoWizard MSConvert,[36] with TPP unchecked, and the CWT filters for peak picking. .ms2 files are directly imported into LipidA-IDER and analyzed using the default settings (Supporting Information Table S4). Additional details are described in the Supporting Information Methods.

Validation Analysis. The major lipid A from the reference bacterial species, *E. coli* and *P. aeruginosa*, were manually annotated and selected for subsequent analysis. These comprised mono- and diphosphorylated lipid A with four to six acyl chains for *E. coli* and mono- and diphosphorylated penta-acylated lipid A for *P. aeruginosa* to account for structural variation. To evaluate the effect of CE on fragmentation profiles, data acquired using CE ranging from 40 to 110 V were used. Acquisition was performed without exclusion time, and therefore for each ion, multiple MS^2 can be acquired. The highest signal for each extracted ion is first evaluated to check for correctness of identification generated by LipidA-IDER, followed by randomizing the ion intensity with bootstrapping (n = 100) to generate a set of spectra with varying number of diagnostic peaks to test the accuracy of LipidA-IDER. The accuracy of the identity assignment was further assessed using all acquired MS^2 data points which vary in quality, and the data are analyzed to determine an optimal score cutoff for subsequent analysis. A total of 27 data sets were used.

Analysis with MS-DIAL. The .wiff files were imported directly into MS-DIAL v4.80.[26] For benchmarking of LipidA-IDER performance, the LipidBlast-neg library[23] and spectral library generated using LipidA-IDER were used. For relative quantitation, lipid A were identified with LipidA-IDER-generated library, and LOWESS correction was applied (refer to Supporting Information Table S5 for MS-DIAL settings used).

Evaluation of LipidA-IDER-Annotated Lipid A from *E. coli* and ESKAPE Pathogens and Spectral Library Generation. MS^2 data were analyzed independently for each strain with LipidA-IDER. In total, 298 data sets were analyzed. Identified features with output scores above the defined score threshold (35) with at least 3 occurrences across all acquisitions per organism were evaluated. When score distance between two hits is less than 15% difference, the data will be evaluated for the presence of coeluting isomers. For identified features with only one occurrence, it will only be accepted if it is acquired using the MS^2 mode and manually reviewed. For identified features with scores above the threshold and lipid A with conflicting identified features, multiple spectra from different acquisitions were manually inspected to confirm the identification. The annotated features for each bacterial species were selected for generation of a spectral library in the .msp format (Supporting Information 2).

Hierarchical Clustering and Heatmap Visualization of Lipid A Features of *E. coli* and Gram-Negative ESKAPE Members. Identified lipid A in each strain were grouped by their structural characteristics. For each characteristic, total count of all lipid A identified that matched the characteristic was normalized to the total number of lipid A identified within each bacterial strain, with exception for the carbon number characteristic, which was normalized to the total number of FA chains present in all lipid A annotated. Hierarchical clustering with Euclidean distance and complete linkage was performed, and the data were visualized with a heatmap (pheatmap, R).

Statistical Analysis. To evaluate the reproducibility of LipidA-IDER, coefficient of variance (CV) of the highest score for each technical replicate from four analytical batches was calculated.

To compare lipid A species/subclass levels between PMX-sensitive and PMX-resistant *A. baumannii* strains, two biological replicates were analyzed. Data presented are a representative set, within which three cultures were sampled per strain, and each lipid A extract was analyzed twice. The data were computed as follows:

$$\text{Ratio of characteristic feature A: B} = \frac{\sum \textit{characteristic feature A}}{\sum \textit{characteristic feature B}}$$

$$\text{Average ratio of characteristic feature A: B} = \bar{X}(\text{ratio of 3 cultures})$$

Fold change of characteristic ratios between two strains were computed, and statistical analysis was performed using Student's t-test. Data were considered significant if p-value is <0.05 and absolute fold change >1.5, and reproduced in the two independent data sets. Bubble plots were constructed with matplotlib in Python.

RESULTS

Lipid A Structure, Fragmentation, and Proposed Nomenclature. Numerous studies demonstrated the feasibility to determine the complex structure of lipid A using negative ESI-MS^2 with collision-induced dissociation (CID)[37−41] (for additional references, refer to Supporting information Tables S1 and S2). Figure 1A shows the general annotation of lipid A structure for simple and intuitive assignment of MS^2 fragment ions generated in this work. The glycan-linked backbone fragment nomenclature was adopted from Domon and Costello.[42]

A three-level classification, summarized in Figure 1B, is used to standardize the nomenclature of lipid A identified with MS^2, in line with recommendations by the lipidomics community.[43,44] Specifically, level 1 entails only the type of headgroup. Level 2 represents the sum composition of the FA and headgroup modifications, and level 3 identification provides higher structural resolution where the position of the fatty acids on the diglucosamine backbone and the chain compositions are defined.

LipidA-IDER Development and Workflow. We designed LipidA-IDER, an automated spectral annotation tool for comprehensive MS^2-based identification of lipid A, in Python. LipidA-IDER can be utilized with a graphical user interface (GUI) or command lines, with user-editable options (available at: https://github.com/Systems-Biology-Of-Lipid-Metabolism-Lab/LipidA-IDER). The architecture of LipidA-IDER consists of two customizable *in silico* libraries and a comprehensive set of fragmentation rules to model the fragmentation of diverse lipid A structures. The building block library (BBLib) is a simple database of headgroups and FA-related ions, theoretically derived from their molecular formulae (Supporting Information Table S6). The theoretical backbone fragment library (TFLib) is a group of known fragment types associated with fragmentation

https://doi.org/10.1021/acs.analchem.1c03566
Anal. Chem. 2023, 95, 602−611

A

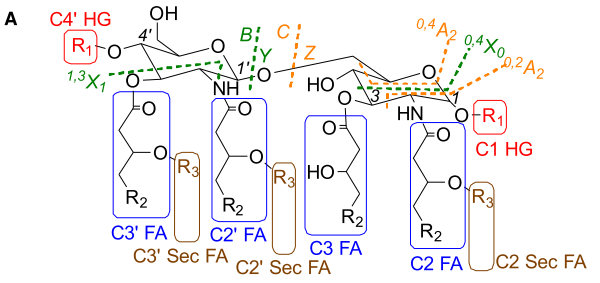

B

Level	Detail	Example: *E. coli* lipid A with *m/z* 1716.25, Ec-43
1	Lipid A subtype identified, sum composition of HG	Monophosphoryl diglucosamine lipid A
2	Sum composition of FA and HG identified	Lipid A hexa-acyl monophosphoryl diglucosamine [P/6/82/0/4]
3	Composition and position of FA and HG identified **Type A:** Resolved position **Type B:** Partially resolved position. Require further experimental confirmation*	Lipid A hexa-acyl C4'-monophosphoryl diglucosamine [P-C14:0_(OH)/C14:0-C14:0_(OH)/C12:0-C14:0_(OH)-C14:0_(OH)/NIL-NIL]

C

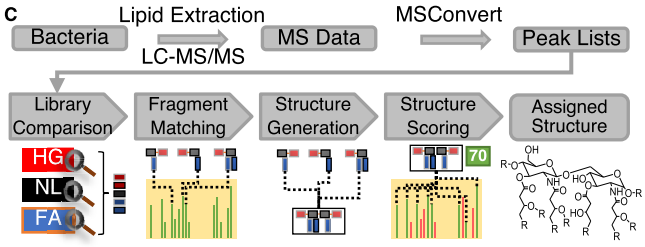

Figure 1. General structure, fragmentation and nomenclature of lipid A, and workflow of LipidA-IDER. (A) Structure of lipid A. HG = headgroup, FA = fatty acyl, R1 = headgroup, R2 = alkyl chain, and R3 = H or acyl chain. Primary FAs (blue box) are linked to the diglucosamine moiety with an amide bond at C2′ and C2 or an ester bond at C3′ and C3. Secondary FAs (brown box) are linked to primary FAs through ester bonds. The C1 and C4′ positions can be modified with different HGs, i.e., different degrees of phosphorylation with addition of PEtN, hexosamines, and Ara4N (not exhaustive) (red box). Using negative ESI-MS^2 with CID, fragmentation can occur at various positions on the diglucosamine backbone (orange and green dashed lines), HG, and FA (as a ketene or acid molecule). (B) Nomenclature of lipid A in this study. Lipid A is annotated with a three-level classification based on the degree of structural resolution. Positions that are not filled are marked with "NIL". In cases where isomers are present confounding the annotation, subcategorization to type A and B will be applied. (C) Schematic of LipidA-IDER, an automated fragmentation-rule-based workflow.

of the diglucosamine backbone (Supporting Information Figure S1 and Table S7).

An extensive set of fragmentation rules for singly deprotonated ($[M-H]^-$) lipid A was derived from a detailed literature review (Supporting Information Tables S1 and S2) and experimentally generated MS^2 data from purified mono- and diphosphorylated lipid A fractions from *E. coli* F583 Rd mutant and biological extracts from *E. coli* and *P. aeruginosa* (Supporting Information Figures S2−S6). These two bacterial species served as a reference to overcome the limitations of the lack of lipid A standards considering their structures and biochemistry are well-established.[5,45] Furthermore, the structural and biochemical differences between the lipid A from *E. coli*[37,46] and *P. aeruginosa*[47,48] provided a source of chemical diversity (Supporting information Figure S7) and enabled the derivation of organism-independent fragmentation rules.

The workflow of LipidA-IDER is summarized in Figure 1C. LipidA-IDER first scans each MS^2 peak list for (i) neutral loss of FAs and headgroups and, (ii) headgroup anions by matching against BBLib (Supporting Information Table S6). Based on this output, a set of backbone fragments using TFLib is generated (Supporting Information Figure S1 and Table S7), which the MS^2 peak list is matched against. Proposed lipid A structures are then constructed using the information inferred from the matched backbone fragments. Subsequently, for each structure, a set of theoretical fragments is generated with the encoded fragmentation rules. As a final step, the MS^2 peak list is matched against each theoretical fragment set. A score is computed based on the sum intensities of matched fragments[19,24] and weighed according to the total input signal and the nature of the fragment ions. LipidA-IDER also calculates the score differences between the top proposed structures as a measure of the confidence of identity matching[18] and as a proxy to evaluate the presence of coeluting isomers.

Accurate identification is crucial for downstream pathway analyses involving specific enzymes[5] (Supporting Information Figure S7). To improve the stringency of identification and to reduce artifacts, LipidA-IDER has additional filtering features as follows: (i) peak intensity cutoff to remove low abundant signals, (ii) minimal number of diagnostic peaks detected, and (iii) biochemical filter to remove structures that do not fit any known substrate constraints of the hydrocarbon rulers, LpxA and LpxD.[49,50] The final output also includes matches to user-defined enzymes linked to the structures to facilitate a biochemistry-driven data review.

Overall, our stepwise, data-driven approach enabled fast and accurate lipid A identification, which took about 40 min to extract and analyze a typical DDA data file (with ∼2717 MS^2-spectra) on a workstation (16GB RAM, 8 core processor) with multiprocessing.

Systematic Evaluation and Validation of LipidA-IDER. Tandem-MS-based identification depends on multiple factors that influence spectral quality, including collision energy (CE) and signal abundance. To evaluate the effect of spectral quality on the accuracy of identification using LipidA-IDER, we analyzed a set of major lipid A species from *E. coli* and *P. aeruginosa* (Figure 2A). LipidA-IDER accurately identified these characterized lipid A over a range of CE when the most abundant signal for each lipid A was evaluated. The score output in general depends on the combination of spectral quality and the number of matched diagnostic ions (Supporting Information Figures S8A,B and S9A,B). To assess the effects of signal intensity of fragment ions and availability of diagnostic peaks on identification, the best hit for each major lipid A was selected for randomization of fragment intensity with bootstrapping (n = 100 for 10 features). Since LipidA-IDER requires data with sufficient diagnostics peaks and intensity for identification, we anticipated that no annotations will be generated when such criterion fail. Indeed, analysis of the signal-randomized data using LipidA-IDER resulted in a 0.91% false positive rate, with the majority of the data (99%) having no annotation (Figure 2B).

To further evaluate the performance of LipidA-IDER and to determine the score threshold for accurate identification of experimental data with mixed quality, all acquired MS^2 features for ions with m/z corresponding to these characterized lipid A were analyzed. The output was assigned to a confusion matrix (Supporting Information Figure S10), and Figure 3C shows the receiver operating characteristic (ROC) curve derived using the

https://doi.org/10.1021/acs.analchem.1c03566
Anal. Chem. 2023, 95, 602−611

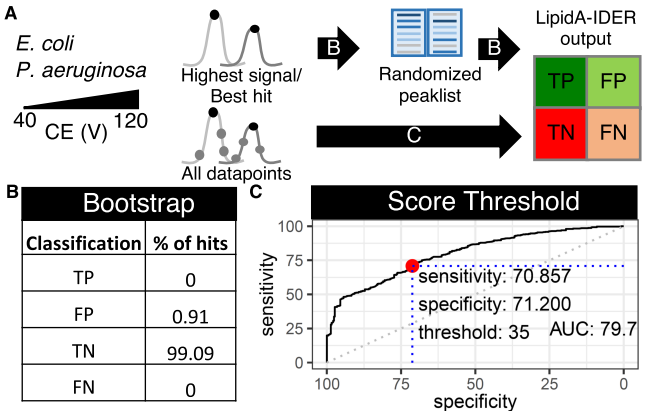

Figure 2. Validation of LipidA-IDER for confident lipid A identification. (A) Schematics of data used for validation. MS^2 data (multiple CE) of major lipid A from *E. coli and P. aeruginosa* were analyzed. The intensity of fragment ions for each of these lipids (arrow B) was randomized to test the performance of LipidA-IDER. All data points acquired in this data set were further analyzed to evaluate the performance of identification for data with mixed quality (arrow C). (B) False positive rate of identification using data with randomized signals (bootstrap n=100). (C) Receiver operator curve (ROC) for determination of the score threshold (in red) for accurate identification of mono- and diphosphorylated lipid A in biological extracts.

final scores to establish a cutoff to balance between sensitivity and specificity of identification. Overall, at a score threshold of 35 (red dot and blue dotted lines), the sensitivity and specificity of LipidA-IDER are 70.9 and 71.2%, respectively (Figure 3C), and this cutoff was chosen for subsequent analysis. It was in general observed that misassignments are more common for low abundant species and peaks with coeluting isomers. Hence, a user-defined filter for peak intensity was incorporated. In addition, the score distance between the top hits can be used as a proxy for the existence of coeluting isomers for users to further evaluate the data.

Next, to determine the effect of analytical variations, MS^2 data from four independent LC−MS batches were analyzed. The score variations for the identification of five lipid A from *E. coli* F583 Rd mutant monophosphorylated fraction were low (<10%), confirming the reproducibility of the workflow (Table 1).

Table 1. Reproducibility of LipidA-IDER Generated Annotation of Lipid A across Four Technical Batches

Lipid A	m/z $[M-H]^-$	CV (%) of score
P/3/40/0/2, Ec-6	1053.66	3.6
P/4/54/0/3, Ec-22	1279.85	2.5
P/5/68/0/3, Ec-31	1490.05	1.7
P/5/68/0/4, Ec-32	1506.05	5.1
P/6/82/0/4, Ec-43	1716.25	2.8

Coverage of Lipid A in the Model Organism, *E. coli*. To benchmark LipidA-IDER performance, we characterized lipid A in the model organism, *E. coli*. Feature maps of lipid A identified in *E. coli* F583 Rd mutant (mono- and diphosphorylated fractions), *E. coli* strain W3110, and *E. coli* pathogenic strain EC958 are presented in Figure 3A−D, respectively. In total, 55 potential lipid A species (assigned ID numbers Ec-1 to Ec-55 in Supporting Information Table S9) were resolved at level 3

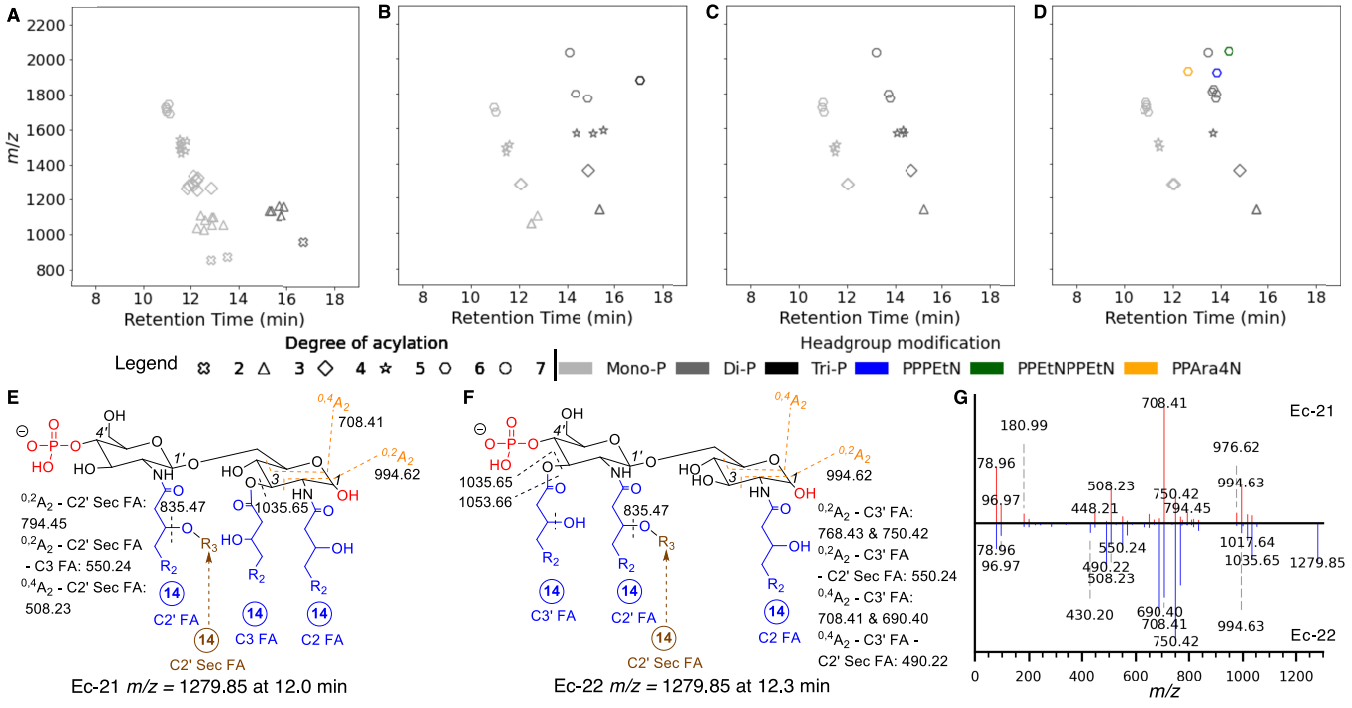

Figure 3. Benchmarking performance of LipidA-IDER for comprehensive identification of *E. coli* lipid A. (A−D) Feature maps of lipid A in *E. coli* F583 Rd mutant monophosphorylated fraction, *E. coli* F583 Rd mutant diphosphorylated fraction, *E. coli* strain W3110, and *E. coli* strain EC958, respectively. Each point represents a unique lipid A structure, where the position represents the retention time and m/z; the color and shape represent the headgroup and degree of acylation, respectively. (E, F) Characterization of monophosphorylated tetra-acylated lipid A with C3′ deacylation (Ec-21, m/z = 1279.85 @ 12.0 min) and its isomer with C3 deacylation (Ec-22, m/z = 1279.85 @ 12.3 min). (G) MS^2 spectra of Ec-21 (top) and Ec-22 (bottom). R2 = alkyl chain and R3 = FA chain. Circled number indicates the carbon number of the FA.

https://doi.org/10.1021/acs.analchem.1c03566
Anal. Chem. 2023, 95, 602−611

identification, in contrast to 44 lipid A with a similar or higher level of structural resolution reported previously.[28,37,40,46] Besides mono-, di-, and triphosphorylated lipid A, PEtN (Ec-52, Ec-55) and Ara4N (Ec-53) modifications were detected in *E. coli* strain EC958, a globally disseminated virulent and multidrug-resistant *E. coli* O 25b:H4-ST131 clone[51] (Figure 3D).

Variations from the classical hydrophobic components were observed in minor lipid A forms, including (i) myristoylation at the C2 secondary position (Ec-40)[37] and (ii) incorporation of an unsaturated C16:1 secondary FA chain at the C2′ position (Ec-26, Ec-35).[40] LipidA-IDER also differentiated isomers with different acylation positions (Figure 3E,F) based on their distinct fragmentation patterns (Figure 3G). For instance, the remodeling lipid A forms, tetra-acylated lipid A deacylated at the C3′ position (Ec-21) and C3 position (Ec-22) were identified, and the structures were corroborated by Sandor and co-workers.[37] In addition, four pairs of potential coeluting isomers were also found (Supporting Information Tables S8 and S9).

Using the data set generated, we next compared the coverage of LipidA-IDER with MS-DIAL[26] using LipidBlast,[23] focusing on diphosphorylated, hexa-acylated lipid A, the only forms in LipidBlast. Although the number of hits was comparable between LipidA-IDER and MS-DIAL/LipidBlast (Table 2),

Table 2. Number of Diphosphorylated (diP) Lipid A Species in *E. coli* Samples Identified Using LipidA-IDER and MS-DIAL

analysis pipeline	*E. coli*/lipid A type	F583 Rd mutant diP	W3110	EC958
LipidA-IDER	diP	8	2	1
	hexa-acyl diP	2	1	1
MS-DIAL/LipidBlast[a]	hexa-acyl diP	3[b]	1[b]	0
MS-DIAL/LipidA-IDER library	diP	7	3	4
	hexa-acyl diP	2	1	1

[a]Score cutoff of 75. [b]Identity of these features was misassigned.

the FA composition of the top hits from the latter was misassigned (Supporting Information Figure S11A). Notably, the reference spectra from LipidBlast lacked diglucosamine backbone fragments (Supporting Information Figure S11B,C), which are critical for accurate assignment of lipid A.[33,52] To improve the spectral similarity-based identification with MS-DIAL, a library was generated from LipidA-IDER-annotated experimental spectra (Supporting Information Figure S11D and Supporting Information 2). Overall, integration of a LipidA-IDER-annotated library resulted in an increase in the numbers, types, and accuracy of lipid A identified with MS-DIAL (Table 2).

Generation of Lipid A Atlas for Gram-Negative Members of ESKAPE Pathogens Using LipidA-IDER Revealed Species- and Strain-Dependent Structural Variants. To demonstrate the general utility of LipidA-IDER for lipid A identification across diverse bacterial species, we analyzed lipid A of Gram-negative ESKAPE pathogens—*Enterobacter hormaechei* (*Enterobacter cloacae* complex), *K. pneumoniae*, *A. baumannii*, and *P. aeruginosa*. *Klebsiella aerogenes*, a nosocomial and pathogenic species, was included to determine species variations within Enterobacteriaceae. LipidA-IDER generated the most comprehensive high-resolution biochemical atlas of lipid A characterized in these medically relevant pathogens. Figure 4A shows the chemical space of lipid A from all six bacterial species. In total, 218 potential lipid A species with 188 distinct structures were annotated in this single study (Supporting Information Tables S8 and S9),with several structures corroborated by earlier studies.[28,29,33,37,40,46−48,53−62]

Clear bacterial species and strain differences were observed when hierarchical clustering was performed on lipid A characteristics profiles (Figure 4B). The Enterobacteriaceae (*E. coli*, *Klebsiella* species, and *E. hormaechei*) shared greater similarity and separated from *A. baumannii* and *P. aeruginosa*. This distinction stemmed primarily from the frequency of hexa-acylated forms of lipid A, with C14:0 FA as the major hydrophobic component. *A. baumannii* and *P. aeruginosa*, on the other hand, formed distinct clusters, where the former was enriched in hepta-acylated lipid A with C14:0 and C12:0 as the major FA components, while the latter was enriched in penta-acylated lipid A with C12:0 and C10:0 as the major FA components.

Remarkable differences were also observed between different strains of the same bacterial species. For both *E. coli* and *K. pneumoniae*, a laboratory strain and a multidrug-resistant (MDR) human isolate were analyzed. Strikingly, in both organisms, modifications of the headgroups with PEtN (Ec-52 and -55) and Ara4N (Ec-53 and Kp-6, -8, -13, -14, -17, -18) were found in the MDR strains, *E. coli* EC958 and *K. pneumoniae* VA360, respectively. Yet, these strains do not carry any known resistance genes or plasmids for PMX.[51,63] Similarly, the MDR *K. aerogenes* strain, UCI15, also possessed a significant number of Ara4N-modified lipid A (Ka-2, -3, -7, -9 -10, -14, -16 to -21), despite its colistin sensitivity (data not shown). Our data suggested that multiple lipid A structural features are potentially linked to PMX resistance. Indeed, it was previously shown that the attachment of Ara4N to lipid A and the subsequent resistance to PMX depend on the presence of the secondary linked myristoylation.[64]

To unravel the fine structural characteristics of PMX-resistant bacteria, we systematically compared the relative levels of lipid A of a pair of *A. baumannii* PMX-sensitive (Ab PRE1) and PMX-resistant (Ab POST1) clinical isolates derived from the same patient.[65] As expected, PEtN-modified lipid A was detected in Ab POST1 (Figure 4B), which harbored mutations in *pmr*B,[65] a two-component sensor kinase signal peptide involved in regulation of PEtN transferase.[66] In addition, when comparing the relative levels of lipid A by structural characteristics, Ab POST1 showed an enriched proportion of lipid A with higher degree of acylation (Figure 4C). Collectively, our data demonstrated that the PMX-sensitive and PMX-resistant *A. baumannii* isolates were distinguished by a combination of the types and relative levels of distinct lipid A species, besides the PEtN-modification arising from known genetic mutations.

DISCUSSION

We present LipidA-IDER, an automated identification tool for lipid A, a class of bacterial lipids which are functionally important for virulence and AMR. LipidA-IDER's extensively curated fragmentation rules and building block libraries can be expanded by users to other lipid A types. In addition, several modifiable settings allow for extensive filtering at different levels of processing to remove redundant lipid identifications and spurious features. Finally, with the acquisition time of a typical LC−MS-DDA analysis of less than 25 min and processing of over 2000 extracted MS^2 spectra within 40 min, LipidA-IDER offers a rapid approach for structural annotation of lipid A from multiple data sets.

https://doi.org/10.1021/acs.analchem.1c03566
Anal. Chem. 2023, 95, 602−611

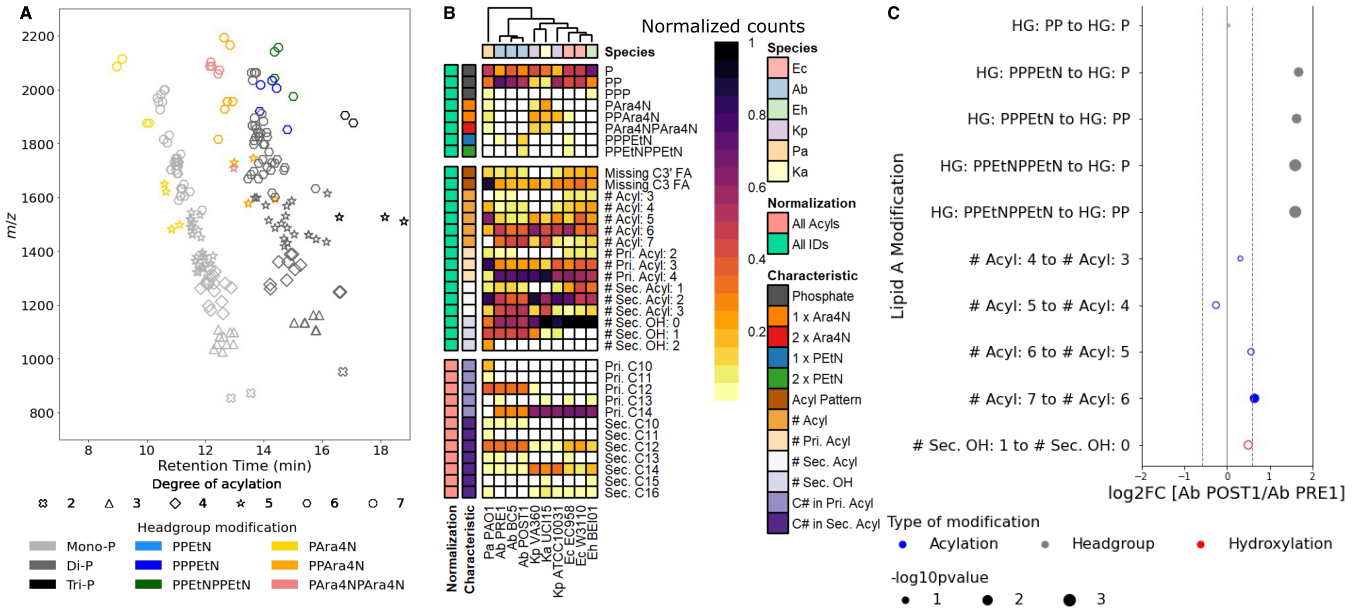

Figure 4. Lipid A repertoire of *E. coli* and Gram-negative ESKAPE pathogens. (A) Combined feature map for lipid A identified at level 3 for *E. coli* and Gram-negative ESKAPE pathogens: *E. coli* (Ec) W3110 and EC958; *E. hormaechei* BEI01; *K. pneumoniae* ATCC10031 and VA360; *K. aerogenes* UCI15; *A. baumannii* BC5, PRE1, and POST1; and *P. aeruginosa* PAO1. Level 3 annotations of these lipid A can be found in Supporting Information Table S9. (B) Heatmap representing the structural characteristics of the identified lipid A in *E. coli* and Gram-negative ESKAPE pathogens. (C) Bubble plot representing the relative changes in lipid A subtypes in *A. baumannii* POST1 compared to *A. baumannii* PRE1. The position and area of the bubbles represent the log2 fold change (log2FC) and p-values, respectively. Only characteristics with significant and reproducible changes are labeled.

LipidA-IDER enables the system-level scale analysis of lipid A in an organism-independent manner, as demonstrated by its application to probe the lipid A repertoire of *E. coli* and Gram-negative members of ESKAPE pathogens. While there is a lack of authenticated standards for lipid A, we harnessed the well-established structures of two bacterial species, *E. coli* and *P. aeruginosa*, to derive the fragmentation rules, which are supported by extensive literature review (Supporting Information Tables S1 and S2). Overall, this is by far the most comprehensive biochemical resource with detailed structural annotation of potential lipid A in these priority pathogens, resolved at the levels of their FA and headgroup composition and positions.

Nonetheless, several limitations of LipidA-IDER which influenced its accuracy exist. First, the lack of resolution of cofragmentation arising from coeluting isobaric lipid A generated mixed spectra which can lead to misidentification. Indeed, we tested LipidA-IDER using infusion-based data generated with both qToF and triple quadrupole MS, and the lack of isomer separation reduced the number of level 3 hits (data not shown). In addition, several lipid A structures can have a high degree of similarity in their fragment profiles, resulting in both false positive and false negative results. For instance, bisphosphorylated and pyrophosphorylated lipid A can be differentiated by the presence of pyrophosphorylation in the cross-ring fragments in the latter form. However, these fragments tend to be low abundant as there is a tendency to lose one phosphate group, leading to misassignment or lack of assignment. Improved resolution of lipid A in complex mixtures can be achieved with chromatographic separation of isomers before MS^2, multistage MS analysis[27] as well as further analysis using doubly charged adducts or positive ionization.[38] Computational approaches for data deconvolution for lipid A need to be developed, which is currently possible for structurally simpler phospholipids enabled by LipiDex.[18] In the current version, LipidA-IDER will generate a flag for lipid A with headgroups which are prone to such misassignment to indicate that the identification is level 3 type B (Figure 1) to prompt users to conduct further verification. In addition, the score distance between top hits can be used as an indicator to screen for existence of coeluting isomers.

Another possible cause of false discovery is the availability of fragmentation rules for different types of lipid A, which can result in misassigned identification, evident from applying the LipidBlast library to our data sets. For the current work, the rule coverage included the $[M - H]^-$ ions for mono-, di-, and triphosphorylated, Ara4N- and PEtN- modified lipid A with diglucosamine backbone and will require further expansion of the fragmentation rules for other lipid A types[6,7] as well as other adduct types. The current work had focused on singly charged $[M - H]^-$ adducts, which are most commonly reported by different studies[33,37−39,41,67,68] and these studies served as a source of reference for the fragmentation rules as well as supporting evidence of the annotated structures. Nonetheless, we observed that for lipid A with multiple modifications, especially on both sugars, the propensity to form doubly charged ions is higher and warrants further work. The coverage of lipid A species identified also further depends on their natural abundance, as the spectral quality of low abundant lipids is insufficient for detailed annotation. Moreover, lipid A content is influenced by environmental conditions and sites of infection,[69,70] and the span of lipid A will change when bacteria are exposed to different stimuli. Indeed, analytical methods, including extraction and LC−MS analysis, and biological variations are potential reasons for differences in coverage of lipid A reported. We also do not rule out that some of the lipid A identified can arise from in-source fragmentation during LC−MS analysis or break down during extraction due to the heating and hydrolysis steps.[71] Despite these pitfalls, LipidA-IDER enabled a comprehensive and simple approach for lipid A

https://doi.org/10.1021/acs.analchem.1c03566
Anal. Chem. 2023, 95, 602−611

analysis with data generated using common instrumentation. In addition, the output of the annotated lipid A can be integrated with software, including MS-DIAL and MetaboKit, for qualitative analysis and relative quantitation, facilitating studies of lipid A functions in bacterial physiology, virulence, and AMR.

With LipidA-IDER, we revealed both the similarities and differences in the lipid A landscape of *E. coli* and Gram-negative members of ESKAPE pathogens. Our data on the complex lipid A repertoire reinforce the known biochemistry of lipid A, including the strict substrate specificity of the hydrocarbon rulers LpxA and LpxD[49,50] (Supporting Information Figure S7), which limit the range of FA incorporated into lipid A. In addition, we uncovered several lipid A features that suggested the presence of previously uncharacterized enzymatic activities for lipid A biosynthesis and remodeling. These included (a) myristoylation at sites of palmitoylation and (b) presence of C3-deacylated lipid A in *A. baumannii* and the Enterobacteriaceae species, suggesting a PagL-like enzyme activity remained to be discovered in these bacteria.[72] The panel of bacterial species and strains analyzed in this study is part of a reference panel we defined, with genome sequences available.[63,73,74] The lipid A atlas generated can thus be integrated with genomics, genetics, and biochemical studies to unravel novel enzymes involved in lipid A metabolism.

Indeed, the detection and characterization of diverse lipid A in this work highlight the natural diversity and complexity of lipid A in biological systems. This is exemplified by our findings on the incorporation of Ara4N and PEtN in bacterial species and strains which are sensitive to PMX. No doubt numerous studies had proven the link between the addition of polar groups to lipid A with PMX resistance at the genetic and biochemical levels.[75] We do not rule out the involvement of transcriptional or post-translational events linked to the presence of modified lipid A in the PMX-sensitive strains. In addition, we demonstrated using a pair of PMX-sensitive and PMX-resistant *A. baumannii* isolates that the latter displayed multiple modifications in lipid A. Specifically, the major modifications of lipid A related to PMX resistance, including addition of PEtN,[33] increased acylation,[59] and hydroxylation of secondary FA,[31] were identified in a single experiment using LipidA-IDER.

In summary, we propose LipidA-IDER as a useful tool for comprehensive lipid A analysis across diverse bacterial species. Moreover, circulating strains have evolved and displayed different lipid A on their outer membranes to adapt to varying environments and we demonstrated the application of LipidA-IDER for comparative lipidomics of MDR and PMX-resistant bacterial strains. A tool that is easily accessible is also of important consideration. Hence, LipidA-IDER was established to interpret MS^2 data generated by common ESI instruments with CID and its output can be integrated with other lipidomics software for downstream data processing. We hope that LipidA-IDER and the lipid A atlas generated will be a useful resource for future studies to uncover novel insights in lipid A metabolism and functions in diverse Gram-negative bacteria.

■ ASSOCIATED CONTENT

Supporting Information

The Supporting Information is available free of charge at https://pubs.acs.org/doi/10.1021/acs.analchem.1c03566.

Supporting Information 1: Supplementary methods; general structure of the backbone generated from fragmentation of the diglucosamine moiety used to build the TFLib (Figure S1); characterization of mono-, di-, and triphosphorylated lipid A in *E. coli* F583 Rd mutant, Ara4N-modified lipid A found in *P. aeruginosa* PAO1, and PEtN-modified lipid A in *E. coli* EC958 (Figures S2−S6); lipid A biosynthesis (Raetz pathway) and modifications found in Gram-negative bacteria (Figure S7); identification of major *E. coli* and *P. aeruginosa* mono- and diphosphorylated lipid A using different collision energy (Figures S8 and S9); classification of lipid A identification output (with a score cutoff of 35) for major mono- and diphosphorylated lipid A from *E. coli* and *P. aeruginosa* (Figure S10); lipid A identification using MS-DIAL (Figure S11); characterization of the structure of lipid A with mass spectrometry in the literature (Table S1); fragment types observed in negative mode CID for various types of lipid A (Table S2); terminology used in LipidA-IDER fragmentation rules (Table S3); settings used in LipidA-IDER and MS-DIAL (Tables S4 and S5); default FA and headgroup BBLib (Table S6); components of the TFLib (Table S7); total number of annotated lipid A (Table S8); and potential lipid A in various bacterial species annotated by LipidA-IDER (Table S9) (PDF)

Supporting Information 2: Experimentally derived lipid A MS^2 spectral library for all organisms analyzed in this study, generated by LipidA-IDER, in the .msp format (ZIP)

■ AUTHOR INFORMATION

Corresponding Author

Xue Li Guan − *Lee Kong Chian School of Medicine, Nanyang Technological University, Singapore 636921, Singapore;* orcid.org/0000-0002-5189-8178; Phone: +65 6592 3957; Email: xueli.guan@ntu.edu.sg

Authors

Johnathan Yi-Xiong Loh − *Lee Kong Chian School of Medicine, Nanyang Technological University, Singapore 636921, Singapore;* orcid.org/0000-0001-8176-0498

Marco Lizwan − *Lee Kong Chian School of Medicine, Nanyang Technological University, Singapore 636921, Singapore*

Sharon Cui Mun Chan − *Lee Kong Chian School of Medicine, Nanyang Technological University, Singapore 636921, Singapore*

Jeric Mun Chung Kwan − *Lee Kong Chian School of Medicine, Nanyang Technological University, Singapore 636921, Singapore;* orcid.org/0000-0002-1310-5464

Tze Peng Lim − *Department of Pharmacy, Singapore General Hospital, Singapore 169608, Singapore*

Tse Hsien Koh − *Department of Microbiology, Singapore General Hospital, Singapore 169608, Singapore*

Li-Yang Hsu − *Saw Swee Hock School of Public Health, National University of Singapore, Singapore 117549, Singapore*

Bernett Teck Kwong Lee − *Lee Kong Chian School of Medicine, Nanyang Technological University, Singapore 636921, Singapore; Centre for Biomedical Informatics, Lee Kong Chian School of Medicine, Nanyang Technological University, Singapore 636921, Singapore; Singapore Immunology Network (SIgN), Agency for Science, Technology and Research (A*STAR), Singapore 138648, Singapore*

Complete contact information is available at:

https://doi.org/10.1021/acs.analchem.1c03566
Anal. Chem. 2023, 95, 602−611

https://pubs.acs.org/10.1021/acs.analchem.1c03566

Author Contributions

Conceptualization, optimization of extraction and LC−MS analysis, data analysis and interpretations, writing, reviewing and editing of the manuscript, funding acquisition: X.L.G.; coding and validation, data analysis and interpretations, and writing and reviewing of the manuscript: J.Y.-X.L. and B.T.K.L. Microbiology, lipid extraction and LC−MS, and literature and manuscript review: M.L. Microbiology and initial manuscript review: S.C.M.C. Pilot coding, preliminary analysis, and initial literature and manuscript review: J.M.C.K. Clinical microbiology of *A. baumannii* isolates and manuscript review: L.H., T.P.L., and T.H.K. All authors have given approval to the final version of the article.

Notes

The authors declare no competing financial interest.

■ ACKNOWLEDGMENTS

This work was supported by the Nanyang Assistant Professorship from Lee Kong Chian School of Medicine, Nanyang Technological University (NTU), and the Ministry of Education (MOE) Tier 2 grant (MOE2017-T2-1-042), awarded to X.L.G. The authors thank Asst. Prof. Marie Loh (NTU) for helpful discussions on statistical validation; Assoc. Prof. Hyung Won Choi and Dr. Guoshou Teo (National University of Singapore, NUS) for their support on MetaboKit; and Assoc. Prof. Shu-Sin Chng (NUS), Asst. Prof. Chris Sham (NUS), and Prof. Howard Riezman (University of Geneva) for their feedback on the manuscript. The following were obtained through BEI Resources, NIAID, NIH: *K. pneumoniae*, strain VA360, NR-48977; *A. baumannii*, strain BC5, NR-17783; *E. hormaechei*, strain BEI01, NR-50391; and *K. aerogenes*, strain UCI15, NR-48555.

■ REFERENCES

(1) May, K. L.; Grabowicz, M. *Proc. Natl. Acad. Sci. U.S.A.* **2018**, *115*, 8852−8854.
(2) Medearis, D. N.; Camitta, B. M.; Heath, E. C. *J. Exp. Med.* **1968**, *128*, 399−414.
(3) Raetz, C. R. H.; Whitfield, C. *Annu. Rev. Biochem.* **2002**, *71*, 635−700.
(4) Needham, B. D.; Trent, M. S. *Nat. Rev. Microbiol.* **2013**, *11*, 467−481.
(5) Raetz, C. R. H.; Reynolds, C. M.; Trent, M. S.; Bishop, R. E. *Annu. Rev. Biochem.* **2007**, *76*, 295−329.
(6) Que-Gewirth, N. L.; Lin, S.; Cotter, R. J.; Raetz, C. R. *J. Biol. Chem.* **2003**, *278*, 12109−12119.
(7) Zamlynska, K.; Komaniecka, I.; Zebracki, K.; Mazur, A.; Sroka-Bartnicka, A.; Choma, A. *Antonie van Leeuwenhoek* **2017**, *110*, 1413−1433.
(8) Needham, B. D.; Carroll, S. M.; Giles, D. K.; Georgiou, G.; Whiteley, M.; Trent, M. S. *Proc. Natl. Acad. Sci. U.S.A.* **2013**, *110*, 1464−1469.
(9) Park, B. S.; Song, D. H.; Kim, H. M.; Choi, B. S.; Lee, H.; Lee, J. O. *Nature* **2009**, *458*, 1191−1195.
(10) Xiao, X.; Sankaranarayanan, K.; Khosla, C. *Curr. Opin. Chem. Biol.* **2017**, *40*, 127−137.
(11) Bishop, R. E. *Nature* **2020**, *584*, 348−349.
(12) Onishi, H. R.; Pelak, B. A.; Gerckens, L. S.; Silver, L. L.; Kahan, F. M.; Chen, M. H.; Patchett, A. A.; Galloway, S. M.; Hyland, S. A.; Anderson, M. S.; Raetz, C. R. H. *Science* **1996**, *274*, 980−982.
(13) Wyckoff, T. J. O.; Raetz, C. R. H.; Jackman, J. E. *Trends Microbiol.* **1998**, *6*, 154−159.
(14) MacLeod, M. K. L.; McKee, A. S.; David, A.; Wang, J.; Mason, R.; Kappler, J. W.; Marrack, P. *Proc. Natl. Acad. Sci. U.S.A.* **2011**, *108*, 7914−7919.
(15) Mata-Haro, V. V.; Cekic, C.; Martin, M.; Chilton, P. M.; Casella, C. R.; Mitchell, T. C. *Science* **2007**, *316*, 1628−1632.
(16) Koelmel, J. P.; Kroeger, N. M.; Gill, E. L.; Ulmer, C. Z.; Bowden, J. A.; Patterson, R. E.; Yost, R. A.; Garrett, T. J. *J. Am. Soc. Mass Spectrom.* **2017**, *28*, 908−917.
(17) Tsugawa, H.; Cajka, T.; Kind, T.; Ma, Y.; Higgins, B.; Ikeda, K.; Kanazawa, M.; VanderGheynst, J.; Fiehn, O.; Arita, M. *Nat. Methods* **2015**, *12*, 523−526.
(18) Hutchins, P. D.; Russell, J. D.; Coon, J. J. *Cell Syst.* **2018**, *6*, 621−625.
(19) Koelmel, J. P.; Kroeger, N. M.; Ulmer, C. Z.; Bowden, J. A.; Patterson, R. E.; Cochran, J. A.; Beecher, C. W. W.; Garrett, T. J.; Yost, R. A. *BMC Bioinf.* **2017**, *18*, 1−11.
(20) Peng, B.; Kopczynski, D.; Pratt, B. S.; Ejsing, C. S.; Burla, B.; Hermansson, M.; Benke, P. I.; Tan, S. H.; Chan, M. Y.; Torta, F.; Schwudke, D.; Meckelmann, S. W.; Coman, C.; Schmitz, O. J.; MacLean, B.; Manke, M. C.; Borst, O.; Wenk, M. R.; Hoffmann, N.; Ahrends, R. *Nat. Commun.* **2020**, *11*, No. 2057.
(21) Tsugawa, H.; Kind, T.; Nakabayashi, R.; Yukihira, D.; Tanaka, W.; Cajka, T.; Saito, K.; Fiehn, O.; Arita, M. *Anal. Chem.* **2016**, *88*, 7946−7958.
(22) Hartler, J.; Triebl, A.; Ziegl, A.; Trötzmüller, M.; Rechberger, G. N.; Zeleznik, O. A.; Zierler, K. A.; Torta, F.; Cazenave-Gassiot, A.; Wenk, M. R.; Fauland, A.; Wheelock, C. E.; Armando, A. M.; Quehenberger, O.; Zhang, Q.; Wakelam, M. J. O.; Haemmerle, G.; Spener, F.; Köfeler, H. C.; Thallinger, G. G. *Nat. Methods* **2017**, *14*, 1171−1174.
(23) Kind, T.; Liu, K. H.; Lee, D. Y.; Defelice, B.; Meissen, J. K.; Fiehn, O. *Nat. Methods* **2013**, *10*, 755−758.
(24) Kochen, M. A.; Chambers, M. C.; Holman, J. D.; Nesvizhskii, A. I.; Weintraub, S. T.; Belisle, J. T.; Islam, M. N.; Griss, J.; Tabb, D. L. *Anal. Chem.* **2016**, *88*, 5733−5741.
(25) Narayanaswamy, P.; Teo, G.; Ow, J. R.; Lau, A.; Kaldis, P.; Tate, S.; Choi, H. *Mol. Omics* **2020**, *16*, 436−447.
(26) Tsugawa, H.; Ikeda, K.; Takahashi, M.; Satoh, A.; Mori, Y.; Uchino, H.; Okahashi, N.; Yamada, Y.; Tada, I.; Bonini, P.; Higashi, Y.; Okazaki, Y.; Zhou, Z.; Zhu, Z. J.; Koelmel, J.; Cajka, T.; Fiehn, O.; Saito, K.; Arita, M.; Arita, M. *Nat. Biotechnol.* **2020**, *38*, 1159−1163.
(27) Ting, Y. S.; Shaffer, S. A.; Jones, J. W.; Ng, W. V.; Ernst, R. K.; Goodlett, D. R. *J. Am. Soc. Mass Spectrom.* **2011**, *22*, 856−866.
(28) Morrison, L. J.; Parker, W. R.; Holden, D. D.; Henderson, J. C.; Boll, J. M.; Trent, M. S.; Brodbelt, J. S. *Anal. Chem.* **2016**, *88*, 1812−1820.
(29) O'Brien, J. P.; Needham, B. D.; Henderson, J. C.; Nowicki, E. M.; Trent, M. S.; Brodbelt, J. S. *Anal. Chem.* **2014**, *86*, 2138−2145.
(30) Tacconelli, E.; Carrara, E.; Savoldi, A.; Harbarth, S.; Mendelson, M.; Monnet, D. L.; Pulcini, C.; Kahlmeter, G.; Kluytmans, J.; Carmeli, Y.; Ouellette, M.; Outterson, K.; Patel, J.; Cavaleri, M.; Cox, E. M.; Houchens, C. R.; Grayson, M. L.; Hansen, P.; Singh, N.; Theuretzbacher, U.; Magrini, N.; Group, W. P. P. L. W.; et al. *Lancet Infect. Dis.* **2018**, *18*, 318−327.
(31) Bartholomew, T. L.; Kidd, T. J.; Sá Pessoa, J.; Conde Álvarez, R.; Bengoechea, J. A. *Infect. Immun.* **2019**, *87*, e00066-19.
(32) Beceiro, A.; Llobet, E.; Aranda, J.; Bengoechea, J. A.; Doumith, M.; Hornsey, M.; Dhanji, H.; Chart, H.; Bou, G.; Livermore, D. M.; Woodford, N. *Antimicrob. Agents Chemother.* **2011**, *55*, 3370−3379.
(33) Pelletier, M. R.; Casella, L. G.; Jones, J. W.; Adams, M. D.; Zurawski, D. V.; Hazlett, K. R. O.; Doi, Y.; Ernst, R. K. *Antimicrob. Agents Chemother.* **2013**, *57*, 4831−4840.
(34) Bligh, E. G.; Dyer, W. J. *Can. J. Biochem. Physiol.* **1959**, *37*, 911−917.
(35) Caroff, M.; Tacken, A.; Szabó, L. *Carbohydr. Res.* **1988**, *175*, 273−282.
(36) Chambers, M. C.; MacLean, B.; Burke, R.; Amodei, D.; Ruderman, D. L.; Neumann, S.; Gatto, L.; Fischer, B.; Pratt, B.; Egertson, J.; Hoff, K.; Kessner, D.; Tasman, N.; Shulman, N.; Frewen,

B.; Baker, T. A.; Brusniak, M. Y.; Paulse, C.; Creasy, D.; Flashner, L.; Kani, K.; Moulding, C.; Seymour, S. L.; Nuwaysir, L. M.; Lefebvre, B.; Kuhlmann, F.; Roark, J.; Rainer, P.; Detlev, S.; Hemenway, T.; Huhmer, A.; Langridge, J.; Connolly, B.; Chadick, T.; Holly, K.; Eckels, J.; Deutsch, E. W.; Moritz, R. L.; Katz, J. E.; Agus, D. B.; MacCoss, M.; Tabb, D. L.; Mallick, P. *Nat. Biotechnol.* **2012**, *30*, 918−920.
(37) Sándor, V.; Dörnyei, Á.; Makszin, L.; Kilár, F.; Péterfi, Z.; Kocsis, B.; Kilár, A. *J. Mass Spectrom.* **2016**, *51*, 1043−1063.
(38) Sándor, V.; Kilár, A.; Kilár, F.; Kocsis, B.; Dörnyei, Á. *J. Mass Spectrom.* **2018**, *53*, 146−161.
(39) Sándor, V.; Kilár, A.; Kilár, F.; Kocsis, B.; Dörnyei, Á. *J. Mass Spectrom.* **2016**, *51*, 615−628.
(40) Okahashi, N.; Ueda, M.; Matsuda, F.; Arita, M. *Metabolites* **2021**, *11*, 197.
(41) Jones, J. W.; Cohen, I. E.; Tureček, F.; Goodlett, D. R.; Ernst, R. K. *J. Am. Soc. Mass Spectrom.* **2010**, *21*, 785−799.
(42) Domon, B.; Costello, C. E. *Glycoconjugate J.* **1988**, *5*, 397−409.
(43) Liebisch, G.; Vizcaíno, J. A.; Köfeler, H.; Trötzmüller, M.; Griffiths, W. J.; Schmitz, G.; Spener, F.; Wakelam, M. J. O. *J. Lipid Res.* **2013**, *54*, 1523−1530.
(44) Pauling, J. K.; Hermansson, M.; Hartler, J.; Christiansen, K.; Gallego, S. F.; Peng, B.; Ahrends, R.; Ejsing, C. S. *PLoS One* **2017**, *12*, e0188394.
(45) King, J. D.; Kocíncová, D.; Westman, E. L.; Lam, J. S. *Innate Immun.* **2009**, *15*, 261−312.
(46) Froning, M.; Helmer, P. O.; Hayen, H. *Rapid Commun. Mass Spectrom.* **2020**, *34*, e8897.
(47) Bedoux, G.; Vallée-Réhel, K.; Kooistra, O.; Zähringer, U.; Haras, D. *J. Mass Spectrom.* **2004**, *39*, 505−513.
(48) Buré, C.; Le Sénéchal, C.; Macias, L.; Tokarski, C.; Vilain, S.; Brodbelt, J. S. *Anal. Chem.* **2021**, *93*, 4255−4262.
(49) Bartling, C. M.; Raetz, C. R. H. *Biochemistry* **2009**, *48*, 8672−8683.
(50) Williams, A. H.; Raetz, C. R. H. *Proc. Natl. Acad. Sci. U.S.A.* **2007**, *104*, 13543−13550.
(51) Totsika, M.; Beatson, S. A.; Sarkar, S.; Phan, M. D.; Petty, N. K.; Bachmann, N.; Szubert, M.; Sidjabat, H. E.; Paterson, D. L.; Upton, M.; Schembri, M. A. *PLoS One* **2011**, *6*, No. e26578.
(52) Kussak, A.; Weintraub, A. *Anal. Biochem.* **2002**, *307*, 131−137.
(53) Madalinski, G.; Fournier, F.; Wind, F. L.; Afonso, C.; Tabet, J. C. *Int. J. Mass Spectrom.* **2006**, *249-250*, 77−92.
(54) Crittenden, C. M.; Akin, L. D.; Morrison, L. J.; Trent, M. S.; Brodbelt, J. S. *J. Am. Soc. Mass Spectrom.* **2017**, *28*, 1118−1126.
(55) Jo, S. H.; Park, H. G.; Song, W. S.; Kim, S. M.; Kim, E. J.; Yang, Y. H.; Kim, J. S.; Kim, B. G.; Kim, Y. G. *RSC Adv.* **2019**, *9*, 19762−19771.
(56) Henderson, J. C.; O'Brien, J. P.; Brodbelt, J. S.; Trent, M. S. *J. Visualized Exp.* **2013**, No. e50623.
(57) Klein, D. R.; Powers, M. J.; Trent, M. S.; Brodbelt, J. S. *Anal. Chem.* **2019**, *91*, 9608−9615.
(58) Kang, K. N.; Klein, D. R.; Kazi, M. I.; Guérin, F.; Cattoir, V.; Brodbelt, J. S.; Boll, J. M. *Mol. Microbiol.* **2019**, *111*, 1604−1616.
(59) Boll, J. M.; Tucker, A. T.; Klein, D. R.; Beltran, A. M.; Brodbelt, J. S.; Davies, B. W.; Trent, M. S. *mBio* **2015**, *6*, 1−11.
(60) Lee, C.-S.; Kim, Y.-G.; Joo, H.-S.; Kim, B.-G. *J. Mass Spectrom.* **2004**, *39*, 514−525.
(61) Li, Y.; Yoon, S. H.; Wang, X.; Ernst, R. K.; Goodlett, D. R. *Rapid Commun. Mass Spectrom.* **2016**, *30*, 2265−2270.
(62) Crittenden, C. M.; Herrera, C. M.; Williams, P. E.; Ricci, D. P.; Swem, L. R.; Trent, M. S.; Brodbelt, J. S. *Analyst* **2018**, *143*, 3091−3099.
(63) Xie, G.; Ramirez, M. S.; Marshall, S. H.; Hujer, K. M.; Lo, C.-C.; Johnson, S.; Li, P.-E.; Davenport, K.; Endimiani, A.; Bonomo, R. A.; Tolmasky, M. E.; Chain, P. S. G. *Genome Announce.* **2013**, *1*, e00168.
(64) Tran, A. X.; Lester, M. E.; Stead, C. M.; Raetz, C. R. H.; Maskell, D. J.; McGrath, S. C.; Cotter, R. J.; Trent, M. S. *J. Biol. Chem.* **2005**, *280*, 28186−28194.
(65) Lim, T.-P.; Tan, T.-Y.; Lee, W.; Sasikala, S.; Tan, T.-T.; Hsu, L.-Y.; Kwa, A. L. *PLoS One* **2011**, *6*, No. e18485.
(66) Adams, M. D.; Nickel, G. C.; Bajaksouzian, S.; Lavender, H.; Murthy, A. R.; Jacobs, M. R.; Bonomo, R. A. *Antimicrob. Agents Chemother.* **2009**, *53*, 3628−3634.
(67) Jones, J. W.; Shaffer, S. A.; Ernst, R. K.; Goodlett, D. R.; Tureček, F. *Proc. Natl. Acad. Sci. U.S.A.* **2008**, *105*, 12742−12747.
(68) Nowicki, E. M.; O'Brien, J. P.; Brodbelt, J. S.; Trent, M. S. *Mol. Microbiol.* **2014**, *94*, 728−741.
(69) Ernst, R. K.; Moskowitz, S. M.; Emerson, J. C.; Kraig, G. M.; Adams, K. N.; Harvey, M. D.; Ramsey, B.; Speert, D. P.; Burns, J. L.; Miller, S. I. *J. Infect. Dis.* **2007**, *196*, 1088−1092.
(70) Llobet, E.; Martínez-Moliner, V.; Moranta, D.; Dahlström, K. M.; Regueiro, V.; Tomás, A.; Cano, V.; Pérez-Gutiérrez, C.; Frank, C. G.; Fernández-Carrasco, H.; Insua, J. L.; Salminen, T. A.; Garmendia, J.; Bengoechea, J. A. *Proc. Natl. Acad. Sci. U.S.A.* **2015**, *112*, E6369−E6378.
(71) Kilár, A.; Dörnyei, Á.; Kocsis, B. *Mass Spectrom. Rev.* **2013**, *32*, 90−117.
(72) Geurtsen, J.; Steeghs, L.; Hove, J. T.; van der Ley, P.; Tommassen, J. *J. Biol. Chem.* **2005**, *280*, 8248−8259.
(73) Forde, B. M.; Ben Zakour, N. L.; Stanton-Cook, M.; Phan, M.-D.; Totsika, M.; Peters, K. M.; Chan, K. G.; Schembri, M. A.; Upton, M.; Beatson, S. A. *PLoS One* **2014**, *9*, No. e104400.
(74) Wee, S. K.; Chan, S. C. M.; Guan, X. L.; Yap, E. P. H. *Microbiol. Resour. Announce.* **2021**, *10*, e00406.
(75) Zhang, H.; Srinivas, S.; Xu, Y.; Wei, W.; Feng, Y. *Trends Biochem. Sci.* **2019**, *44*, 973−988.

https://doi.org/10.1021/acs.analchem.1c03566
Anal. Chem. 2023, 95, 602−611